Embedded-ion method: An analytical energy-conserving charge-transfer interatomic potential and its application to the La-Br system

X. W. Zhou[1,*] and F. P. Doty[2]
[1]*Department of Mechanics of Materials, Sandia National Laboratories, Livermore, California 94550, USA*
[2]*Department of Engineered Materials, Sandia National Laboratories, Livermore, California 94550, USA*
(Received 16 June 2008; revised manuscript received 11 August 2008; published 12 December 2008)

Molecular-dynamics simulations of ionically bonded material systems with nonstoichiometric composition, interfaces or surfaces, defects, or other local environments that are substantially different from a stoichiometric bulk require the use of a variable charge interatomic potential. In conventional variable charge molecular-dynamics simulations, the charges on atoms are solved by minimizing the system potential energy with respect to charges. The reduced potential energy during this energy minimization process is not accounted for in the force calculation and therefore does not contribute to a corresponding increase in the kinetic energies of atoms. As a result, the total system energy decays over time. This energy nonconserving behavior precludes the method from being used to study problems such as thermal transport and thermal diffusion. It may also lead to inaccurate results for other types of simulations. Here we attempt to overcome this problem by analytically incorporating variable charge concepts into an embedded-ion method, which has mathematical format similar to the well-known embedded-atom method. We illustrate the approach using the La-Br system.

DOI: 10.1103/PhysRevB.78.224307 PACS number(s): 34.20.Cf, 02.70.Ns, 61.50.Lt, 34.70.+e

I. INTRODUCTION

Ionically bonded materials such as halides and oxides have the potential to solve many technologically critical problems that cannot be solved with other material systems. For instance, an oxide layer such as an MgO layer can be used in magnetic tunnel junction multilayers to introduce a spin-dependent electron tunneling effect, which is enabling next generation of random-access memory that is nonvolatile, radiation hard, and energy conservative.[1] Due to correlated electrons,[2,3] many oxide interfaces have been recently found to exhibit special properties such as tunable dielectrics,[4,5] giant thermoelectrics,[6] high interfacial electron mobility,[7] and interfacial superconductivity.[8] These properties are likely to result in ultrasensitive sensors, improved batteries, and next generation of electronic and optic devices with high speed and low power consumption. One material of contemporary interest is $LaBr_3$ used as a viable scintillator material for gamma ray spectroscopy.[9] For this application, a large volume high quality $LaBr_3$ single crystal is desired for maximizing the material interaction with radiation. The yield of large volume crystals that can be grown today, however, is critically limited by $\{11\bar{2}0\}$ cleavage when the crystal volume is grown above a threshold.[10] A grand challenge toward either an enhanced halide scintillator technology or future oxide electronics is the understanding of atomic scale structures of complicated ionically bonded materials and the development of methods to synthesize and control these structures. Large scale atomistic simulations using interatomic potentials are effective in revealing atomic scale structures of materials and, therefore, can help promote many of the technologies mentioned above.[11–13] Atomistic simulations of $LaBr_3$ solid compounds have thus been sought to study the cleavage mechanism and effects, such as stress evolution, dislocation motion, and crystallographic orientation, as well as to explore methods that can strengthen the material to avoid fracture. Review of the literature, however, indicates that no atomistic simulations of $LaBr_3$ solid compounds have been published and the closest work has addressed only the molten phase of the material.[14]

Compared with metallically bonded[11,15–17] and covalently bonded[18–25] systems, interatomic potentials used for ionically bonded systems are less mature.[26] In earlier studies, ionically bonded materials were simulated using a fixed-charge pairwise potential superimposed on an electron shell model.[14,26–34] There are some limitations with the fixed-charge models: (i) they overestimate the cohesive energy of materials by almost four times;[35] (ii) they can only be used to study stoichiometric composition and any other compositions that possess a nonzero system charge will have infinite system energy (under the periodic boundary conditions); and (iii) they cannot be used to study defects such as a metal particle embedded in an oxide matrix, which would require the potential to assign zero charges to atoms that are within the metal particle and maximum charges to atoms that are within the oxide matrix. Recent simulations of ionically bonded materials,[36–38] therefore, have begun to employ variable charge potential models.[35,39–41] In previous numerical variable charge molecular-dynamics (MD) simulations, charges on atoms are solved each time step using an energy minimization algorithm.[35,39,40] Putting aside that this energy minimization can reduce the calculation efficiency by orders of magnitude, a bigger problem is that any energy reduction during this process is not reflected by the force calculations and is not converted to the kinetic energy of atoms. As a result, system energy decays over time. Such a simulation, therefore, cannot be used to study thermal transport and thermal diffusion problems. It may also lead to inaccurate results for other types of simulations. Similar problems also exist in other empirical-MD simulations that use energy minimization without a self-consistent adjustment of forces. The shell model, for instance, minimizes the energy for electron-core polarization without correspondingly adjusting forces.[27–30]

Unlike the empirical-MD approaches, *ab initio*–MD

simulations explicitly include dynamics of electrons in the evolution of atom positions[42] (i.e., the derivative of charges with respect to atom positions is considered in the force calculations). As a result, *ab initio*–MD simulations can in principle ensure energy conservation. In practice, however, energy conservation demands a small convergence tolerance for energy minimization with respect to electronic structure[43] and a time-reversal computational scheme.[44] The use of a small convergence tolerance can significantly increase the computational cost. This problem results in the development of two different types of MD schemes: Born-Oppenheimer methods and extended Lagrangian methods.[42,43,45] In Born-Oppenheimer methods, the electronic structures are fully converged each time step, but the calculations are very expensive. The extended Lagrangian methods seek to propagate the electronic structures without ensuring their full convergence each time step. Although this accelerates the calculations, it introduces errors leading to energy drift.

As in *ab initio*–MD methods, it is possible to incorporate the position dependence of charges into the force calculation in empirical-MD methods. However, this is so computationally demanding that the main advantage of the empirical-MD methods for handling large scale systems is lost. Here we seek to incorporate variable charge concepts into an analytical embedded-ion method (EIM) potential where the equilibrium charges are embedded in the potential so that the energy minimization step is eliminated. Because of this, the method is both energy conserving and computationally efficient. We illustrate the approach by developing a La-Br EIM potential capable of simulating the $LaBr_3$ solid phase compound. $LaBr_3$ is a good example to illustrate the method because it has a relatively complicated crystal structure (hexagonal lattice with local rotation of Br polyhedron surrounding each La atom, a small lattice-constant ratio of $c/a \approx 0.57$, a slightly longer bond length between La and Br cap atoms than that between La and Br prism atoms, and lattice hollows).[46,47]

II. THEORY DEVELOPMENT

In this section, we first describe the experimental criteria for the stability of crystal structure of ionically bonded compounds as a motivation for the variable charge potential. We then discuss why the previous numerical approaches of the variable charge potential have the energy nonconservation problem. After that we lay out the main assumptions behind our analytical EIM model and finally we formulate the potential based on these assumptions.

A. Experimental criteria for crystal structure

The earliest attempt to understand structures of complex ionic crystals was made by Goldschmidt[48] in 1927.[49] This resulted in the well-known Goldschmidt criterion[48] that relates crystal structure of ionic compounds to ionic radii of constituent species. Improved criterion to predict structures was soon elaborated by Pauling[50] in 1939. This new criterion further relates the crystal structure to valence and coordination. Valence and coordination affect crystal structures because when atoms of dissimilar species are brought together, they may induce charges on each other which then change the effective radius of an atom depending on the local environment.[50] The tendency for atoms to become charges has been characterized by a material property called electronegativity.[50–52] The utility of Pauling's criterion[50] stimulates continued research in this area and recent work to extend this empirical relationship to include electronegativity effects has been published.[53]

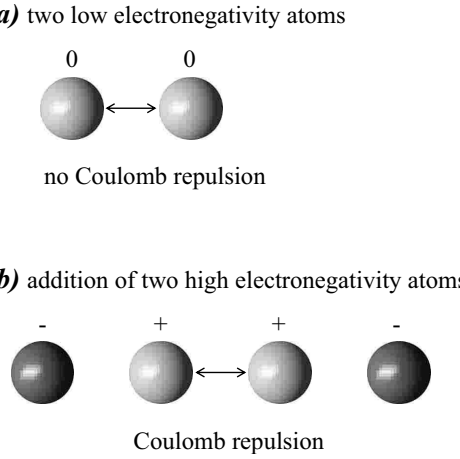

FIG. 1. Schematic illustration of electronegativity on atomic bonding: (a) two similar atoms and (b) two similar and two dissimilar atoms.

By adjusting the atom separation distance at which a potential-energy well occurs, a simple potential-energy model (e.g., pair potential) can capture the effect of ionic radius. The effect of electronegativity is schematically illustrated in Fig. 1. In Fig. 1(a), two atoms with the same electronegativity form a bond. Because the two atoms have the same electronegativity, no charge is induced. As a result, there is no Coulomb repulsive interaction between them. In Fig. 1(b), another two atoms with a higher electronegativity are added to the neighbor of the existing two atoms. Due to the high electronegativity, the added atoms become negatively charged by inducing positive charges on the existing atoms. This introduces a Coulomb repulsive interaction between the two existing atoms. It is this reactive environment dependent atomic bonding that requires the use of a variable charge model.[35,39,40]

B. Origin of energy nonconservation

In variable charge potential models, the total system potential energy, E, is expressed as a function of both atom positions and atom charges,

$$E = E(\mathbf{x}_1, \mathbf{x}_2, \ldots, \mathbf{x}_N, q_1, q_2, \ldots, q_N), \tag{1}$$

where $\mathbf{x}_i$ and q_i are, respectively, position and charge of atom i $(i=1,2,\ldots,N)$ and N is total number of atoms in the system. It is assumed that at any given time, the system always adopts the atomic charges that minimize the potential energy. These atomic charges vary as atoms move. It is this replacement of the fixed charges by the variable charges that contrasts the fixed-charge models.[35]

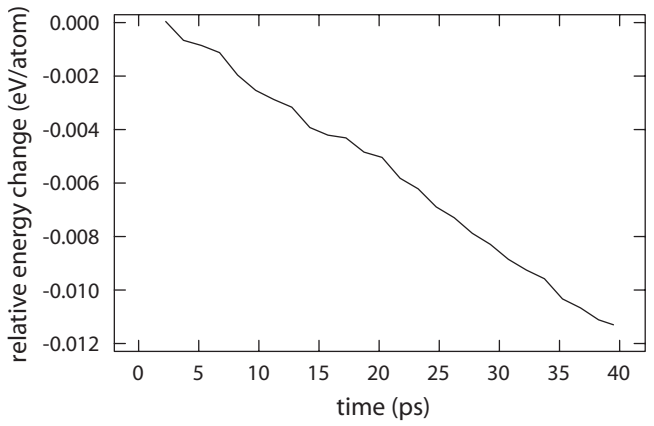

FIG. 2. Relative energy change (per atom) as a function of time predicted by conventional variable charge methods.

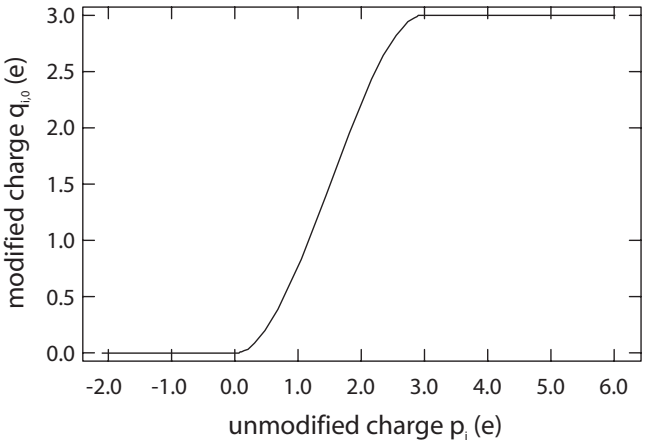

FIG. 3. Relation between unmodified charge (p_i) and modified charge $q_{i,0}$.

Under the charge neutral condition, $\Sigma_{i=1}^{N} q_i = 0$, the N charges, $q_1, q_2, \ldots, q_N$, define only $N-1$ independent variables. Let us assume that q_N depends on $q_1 - q_{N-1}$. The first equation defining equilibrium charges can be expressed as

$$q_N = -\sum_{i=1}^{N-1} q_i. \tag{2}$$

From the minimum-energy condition

$$\begin{aligned} \partial E(q_1, q_2, \ldots, q_{N-1})/\partial q_i &= \partial E(q_1, q_2, \ldots, q_N)/\partial q_i \\ &+ \partial E(q_1, q_2, \ldots, q_N)/\partial q_N \cdot \partial q_N/\partial q_i \\ &= \partial E/\partial q_i - \partial E/\partial q_N = 0, \end{aligned}$$

we can list $N-1$ additional equations,

$$\frac{\partial E}{\partial q_i} = \frac{\partial E}{\partial q_N} \quad (i = 1, 2, \ldots, N-1). \tag{3}$$

Equation (3) can also be viewed as an equal chemical-potential condition.[39,54–56] Equations (2) and (3) completely define the N equilibrium charge parameters.

Previous numerical variable charge MD simulations iterate over three steps:[35,39] (i) solving Eqs. (2) and (3) for charges that minimize the system potential energy; (ii) calculating forces on atoms assuming charges on atoms are fixed at the values determined in (i); and (iii) integrating atom positions using Newton's equation of motion.

It should be recognized that step (ii) described above involves an assumption that the position dependence of charge does not contribute to the force. We can demonstrate that this is true when the charge neutral and minimum-energy conditions [Eqs. (2) and (3)] are satisfied. For instance, the x component of the force on atom i due to the position dependence of charge q can be expressed as

$$f_{x,i}|^q = -\left.\frac{\partial E}{\partial x}\right|^q = -\sum_{i=1}^{N} \frac{\partial E}{\partial q_i}\frac{\partial q_i}{\partial x} = -\frac{\partial E}{\partial q_N}\frac{\partial \sum_{i=1}^{N} q_i}{\partial x} = 0. \tag{4}$$

In practice, however, the minimum-energy condition is only satisfied at the end, but not at the beginning, of step (i). This means that step (i) always results in some energy reduction. This energy reduction is not accounted for in the force calculation described by step (ii) and therefore cannot be converted to a corresponding increase in the kinetic energy of atoms. As a result, the total system energy decays over time during constant energy MD simulation. Note that the problem cannot be solved by reducing the time step size because the charges on atoms are treated as step functions regardless of the time step size and the energy minimization is always needed to cause an abrupt change in energy at the step edge even at an infinitely small time step size (or the method simply reduces to a fixed-charge model).

How quickly the energy decays depends on the potential parameters, time integration scheme, and the simulated problem. As an example, we used a variable charge potential[57] in a constant energy MD simulation to anneal an α-Al_2O_3 bulk containing 120 atoms. The equilibrium system temperature was set at 600 K and a time step size of 0.001 ps was used. At each time step, a fully converged energy minimization was used to solve for the charges. The average relative change in energy (per atom) obtained from this simulation is shown in Fig. 2 as a function of time. Clearly Fig. 2 shows an almost linear decay of the energy by 0.012 eV/atom over a short-time period of only 40 ps.

C. Assumptions

Our approach is based on mainly five assumptions:

(a) The total energy of the system, E, is composed of a non-charge-related energy, E_n, and a charge-related energy, E_q: $E = E_n + E_q$. In particular, $E_q = 0$ when charges q are zero and $E_q \neq 0$ when charges are not zero;

(b) Charges in metallic and covalent systems are zero;

(c) Cation atoms can only lose electrons (to become positive charges) until all their valence electrons are gone, and anion atoms can only acquire electrons (to become negative charges) until their outer electron shells are filled;

(d) The charge-related interactions can be approximated by short-range potential functions; and

(e) Charges on atoms are induced by the valence and electronegativity of neighboring atoms.

Here assumptions (a)–(c) are inherited from the previous variable charge models,[35,39] assumption (d) has been used by the ReaxFF approach,[58] and assumption (e) is slightly modified from the previous concept. Assumption (a) allows the charge-related and non-charge-related energies to be separately treated. Assumption (b) enables the variable charge model for ionically bonded systems to be transferable to those of metallically bonded or covalently bonded systems. This is because it results in a zero charge-related energy E_q in metallic and covalent systems, and the total energy E then becomes equivalent to the energy E_n defined by non-charge-related models. In this sense, E_q can be viewed as the energy change when the metallic or covalent system is transformed to an ionic system (e.g., when the metal is oxidized). It should be noted that strictly speaking, charges on different elements in a metallic alloy or a covalent compound may not be precisely zero. However, the premise is that these charge effects have already been included in the potential E_n. It is in this sense that the zero-charge assumption is required to ensure the transferability of the potential.

Assumption (c) is essentially required by classical physics. Variable charge potentials that do not satisfy this assumption may become divergent at some parameters. They also cannot predict zero charges in metallic alloys or covalent compounds, and as a result, they are transferrable only in binary systems.[35] In the following, we will show that this assumption is critical for our model to predict zero charges in metallic and covalent systems.

Assumption (d) is not required for the model to work. However, it is well known that the slow decaying Coulomb interaction cannot be simply summed up in the normal space for periodic systems.[35] By making the interaction range shorter, the interaction can be directly summed and calculations are significantly simplified. We therefore made this assumption based on several considerations: (i) charges on atoms diminish as atoms are pulled apart, and as a result, ionic interaction decays faster than the $1/r$ decaying rate defined by the fixed-charge Coulomb interaction; (ii) lattice atoms have a strong screening effect so that the interaction range is shorter; and (iii) the long-range Coulomb interaction can be split into $1/r=\mathrm{erfc}(\tau\cdot r)/r+\mathrm{erf}(\tau\cdot r)/r$, where τ is an arbitrary splitting factor. Based on an Ewald summation technique,[59,60] interaction can be separately calculated in the normal space for the short-range function $\mathrm{erfc}(\tau\cdot r)/r$ and in the reciprocal space for the long-range function $\mathrm{erf}(\tau\cdot r)/r$. The long-range contribution can be made relatively insignificant by adjusting the value of τ. Note that the error introduced by the negligence of the long-range interaction can be further reduced through parametrization if the short-range function is more general than $\mathrm{erfc}(\tau\cdot r)/r$.

Assumption (e) simplifies our model. Previous models[35,39,40] essentially assume that charges on atoms depend on charges on the neighboring atoms. Due to a chain reaction, charges must be solved from an $N\times N$ matrix and analytical solution is not feasible when the system contains more than a few atoms. By assuming that charges on atoms depend on the valence and electronegativity of neighboring atoms, the basic charge-transfer physics illustrated in Fig. 1 is still captured and charges can be analytically expressed.

D. Formulation

The charge-related energy is many-body dependent. Our EIM therefore adopts a form similar to that of the well-known embedded-atom method (EAM).[15,16] The total energy of the system is expressed as

$$E=\sum_{i=1}^{N}\sum_{j=i_1}^{i_N}\phi_{ij}(r_{ij})+\sum_{i=1}^{N}E_{\mathrm{emb},i}(\sigma_i), \tag{5}$$

where $\phi_{ij}(r)$ is a pair energy between atoms i and j separated by a distance r, $E_{\mathrm{emb}}(\sigma)$ is the embedding energy arising from embedding an atom i into a local ionic background defined by the quantity σ, N is total number of atoms in the system, and j loops over i's neighbor list $i_1,i_2,\ldots,i_N$. Note that we have assumed $E_n=\Sigma_{i=1}^{N}\Sigma_{j=i_1}^{i_N}\phi_{ij}(r_{ij})$ and $E_q=\Sigma_{i=1}^{N}E_{\mathrm{emb},i}(\sigma_i)$. In the following, we derive the detailed formulism of Eq. (5).

1. Non-charge-related energy E_n

Our simple pair potential function for the non-charge-related energy E_n was designed to capture the atomic radius effects and was expressed as

$$\phi_{ij}(r)=\varphi_{ij}(r)f_{ij}(r), \tag{6}$$

where $f_{ij}(r)$ is a cutoff function which approximately equals 1 when r is much less than the cutoff distance of the potential, $r_{c,ij}$, and smoothly decays to 0 when r approaches $r_{c,ij}$, and $\varphi_{ij}(r)$ is expressed as

$$\varphi_{ij}(r)=\frac{E_{b,ij}\beta_{ij}}{\beta_{ij}-\alpha_{ij}}\exp[-\alpha_{ij}(r-r_{e,ij})]-\frac{E_{b,ij}\alpha_{ij}}{\beta_{ij}-\alpha_{ij}}\exp[-\beta_{ij}(r-r_{e,ij})]. \tag{7}$$

Here $E_{b,ij}$ is the energy well of the $\varphi_{ij}(r)$ function, $r_{e,ij}$ is the atom separation distance at which the energy well occurs, and α_{ij} and β_{ij} are two additional parameters that can freely adjust the shape of the function curve. Note that Eq. (7) is essentially a variation in a generalized Morse potential.

The cutoff function takes the following form:

$$f_{ij}(r)=\frac{\mathrm{erfc}[\kappa_{ij}(r-r_{c,ij}+s/\kappa_{ij})]-\mathrm{erfc}(s)}{2-\mathrm{erfc}(s)}, \tag{8}$$

where parameter κ_{ij} controls the decay rate and decay range of the function and parameter s ensures that the function drops to zero at $r=r_{c,ij}$. Equation (8) is a very smooth cutoff function provided that $\mathrm{erfc}(s)$ is a small number. In the present work, we assumed $s=1.644\,98$, which was solved from equation $\mathrm{erfc}(s)=0.02$. We let only κ_{ij} be the fitting parameter.

Most previous interatomic potentials apply the cutoff function over a designated cutoff range.[61,62] Such potentials do not have continuous second derivative at the starting junction point of the cutoff function. In addition, the cutoff distance usually cannot be treated as a fitting parameter. One advantage of Eq. (6) over most previous approaches is that it has continuous high order derivatives and allows the cutoff distance to be treated as a fitting parameter. It was the tuning

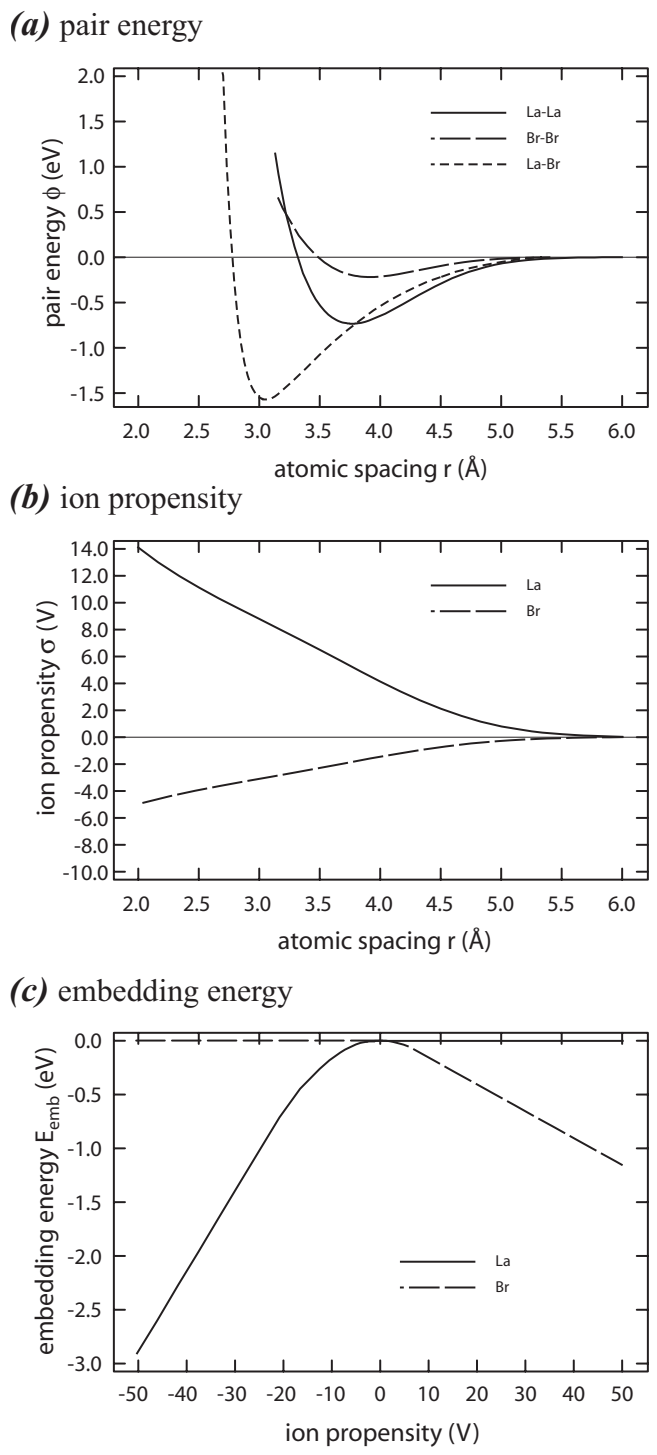

FIG. 4. EIM functions. (a) Pair energy, (b) ion propensity, and (c) embedding energy.

of the cutoff distance that greatly improved the flexibility of our parametrization.

2. Charge-related energy E_q

The main concept of the previous variable charge model[35,39–41] is that charge on an atom arises under balance of three driving forces: electronegativity, self-Coulomb repulsion, and Coulomb interaction. According to the standard

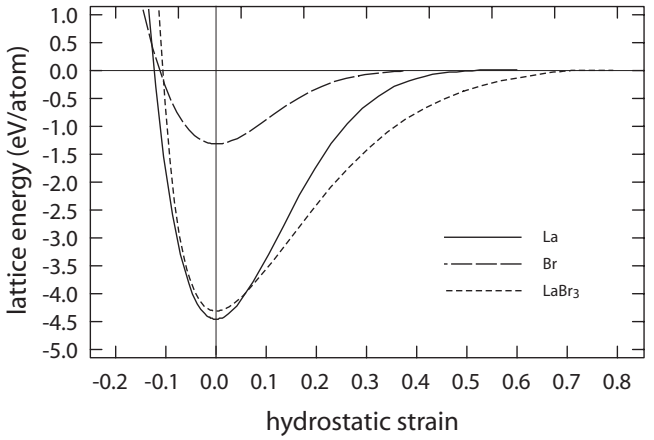

FIG. 5. Energy per atom as a function of hydrostatic strain for the three phases: (fcc) La, (fcc) Br, and (UCl_3) $LaBr_3$.

charge-related energy function,[35,39–41] we have

$$E_q = \sum_{i=1}^{N} E_{\mathrm{emb},i} = \sum_{i=1}^{N} \left(\chi_i \cdot q_i + \frac{1}{2} J_i q_i^2 + \frac{1}{2} \sum_{\substack{j=1 \\ j \neq i}}^{N} k_c \frac{q_j q_i}{r_{ij}} \right), \quad (9)$$

where $k_c = 14.4$ V Å e^{-1} is Coulomb constant, χ_i and J_i are electronegativity and self-Coulomb repulsion coefficient of atom i, and q_i and q_j are charges on atoms i and j. Note that by using charge neutral condition, we can write $\Sigma_{i=1}^{N} \chi_i \cdot q_i = -\Sigma_{i=1}^{N} \Sigma_{\substack{j=1 \\ j \neq i}}^{N} \chi_j \cdot q_i$. Substituting this into Eq. (9), we can write

$$E_{\mathrm{emb},i} = -\sum_{\substack{j=1 \\ j \neq i}}^{N} \chi_j \cdot q_i + \frac{1}{2} J_i q_i^2 + \frac{1}{2} \sum_{\substack{j=1 \\ j \neq i}}^{N} k_c \frac{q_j q_i}{r_{ij}}. \quad (10)$$

Consider the charge q_j on neighbor atoms $j = i_1, i_2, \ldots, i_N$. In general, we can assume that q_j reaches the maximum value when the local environment is close to that in a stoichiometric ionic compound. We can expand q_j in terms of this stoichiometric ionic compound as

$$q_j = Z_j + \frac{\partial q_j}{\partial \eta} \Delta\eta + \frac{1}{2} \frac{\partial^2 q_j}{\partial \eta^2} \Delta\eta^2 + \cdots, \quad (11)$$

where Z_j is valence of atom j (approximated as its maximum charge), η is a measure of local ionic environment, and $\Delta\eta$ represents the deviation of this local ionic environment from that in the stoichiometric compound. We are currently working to incorporate the dependence of q_j on the environment. In this work, we approximately assume that $q_j = Z_j$, which is accurate when $\Delta\eta$ is small and maintains the physics shown in Fig. 1 even when $\Delta\eta$ is large as it is consistent with assumption (e) listed above.

Based on assumption (d) which requires that charge-related interactions to be cut off at a short distance and $q_j = Z_j$, we rewrite Eq. (10) as

$$E_{\mathrm{emb},i} = \zeta_i \left[\sum_{j=i_1}^{i_N} (-\chi_j) \cdot G_j(r_{ij}) \cdot q_i + \frac{1}{2} J_i q_i^2 + \frac{1}{2} \sum_{j=i_1}^{i_N} k_c \frac{Z_j q_i}{r_{ij}} F_j(r_{ij}) \right]. \quad (12)$$

Here the radially decaying localization functions $G_j(r)$ and $F_j(r)$ are introduced to enable the summation to be cut off at a given cutoff distance within which atom i only forms bonds with i_N neighbor atoms, $j=i_1, i_2, \ldots, i_N$, and coefficient ζ_i is currently treated as a fitting parameter to allow our model to be better fitted to properties. Note that $F_j(r)$ is a radially decaying function because of assumption (d). In the original model, $F_j(r)$ would take a value of 1 for point charge and take more complicated radial dependent function form for distributed electron-core structure.[35,39]

For simplicity, we can assume that $G_j(r)=\frac{F_j(r)}{r}$. This equation is not required, but the model does not improve with independent $G(r)$ and $F(r)$ unless there are clear inputs to allow their separate determination. We then have

$$\sum_{j=i_1}^{i_N} (-\chi_j) \cdot G_j(r_{ij}) \cdot q_i + \frac{1}{2} \sum_{j=i_1}^{i_N} k_c \frac{Z_j q_i}{r_{ij}} F_j(r_{ij}) = \sum_{j=i_1}^{i_N} \left(\frac{1}{2} k_c Z_j - \chi_j \right) \frac{F_j(r_{ij})}{r_{ij}} \cdot q_i = \sigma_i \cdot q_i, \quad (13)$$

where

$$\sigma_i = \sum_{j=i_1}^{i_N} \left(\frac{1}{2} k_c Z_j - \chi_j \right) \frac{F_j(r_{ij})}{r_{ij}} = \sum_{j=i_1}^{i_N} \gamma_j \frac{F_j(r_{ij})}{r_{ij}} = \sum_{j=i_1}^{i_N} \sigma_j^a(r_{ij}). \quad (14)$$

Here we can treat $\gamma_j=\frac{1}{2}k_c Z_j-\chi_j$ as a fitting parameter. We can call σ_i the ion propensity at site i because it is this local background quantity that drives the ionization of the embedded atom. Note that unlike the electron density in the EAM model, the ion propensity referred to here can be both negative and positive. A positive-ion propensity tends to induce a negative charge on the embedded atom and a negative-ion propensity tends to induce a positive charge on the embedded atom. It can be seen from Eq. (14) that the atomic contribution to the total ion propensity at site i from atom j that is a distance r away can be expressed as

$$\sigma_j^a(r) = \gamma_j \frac{F_j(r)}{r}. \quad (15)$$

By definition, cations have a positive γ_j value and they create a positive-ion propensity to their surroundings; likewise, anions have a negative γ_j value and they create a negative-ion propensity to their surroundings.

Based on our assumption (d), we can approximate $F_j(r)$ with a general decay function,

$$F_j(r) = \frac{\mathrm{erfc}\lfloor \xi_j (r - r_{c,j}^* + s/\xi_j) \rfloor - \mathrm{erfc}(s)}{2 - \mathrm{erfc}(s)}. \quad (16)$$

Equation (16) is similar to Eq. (8) except that it uses a different cutoff distance $r_{c,j}^*$ and a different decaying parameter ξ_j.

Substituting Eq. (13) into Eq. (12), we have

$$E_{\mathrm{emb},i} = \zeta_i \left(\frac{1}{2} J_i q_i^2 + \sigma_i \cdot q_i \right). \quad (17)$$

The charge p_i that gives minimum embedding energy defined by Eq. (17) can be solved from $\frac{dE_{\mathrm{emb},i}}{dq_i}\big|_{q_i=p_i}=0$, which leads to

$$p_i = -\frac{\sigma_i}{J_i}. \quad (18)$$

Assumption (c) requires that the equilibrium charge of an atom i be bounded between $q_{\min,i}$ and $q_{\max,i}$, where $q_{\min,i}$ and $q_{\max,i}$ correspond to a positive range (with $q_{\min,i}=0$ and $q_{\max,i}>0$) if atom i is a cation and a negative range (with $q_{\min,i}<0$ and $q_{\max,i}=0$) if atom i is an anion. The p_i defined by Eq. (18) may not satisfy this condition. We therefore use the following spline function to cast p_i to a modified equilibrium charge, $q_{i,0}$, which satisfies this condition:

$$q_{i,0} = \begin{cases} q_{\min,i}, & p_i \le q_{\min,i} \\ \dfrac{q_{\min,i}+q_{\max,i}}{2} + g_i \left(p_i - \dfrac{q_{\min,i}+q_{\max,i}}{2} \right) + h_i \left(p_i - \dfrac{q_{\min,i}+q_{\max,i}}{2} \right)^3, & q_{\min,i} < p_i < q_{\max,i} \\ q_{\max,i}, & p_i \ge q_{\max,i}. \end{cases} \quad (19)$$

Here g_i and h_i are two constants that can be determined by requiring the spline function to be smooth. Due to symmetry, g_i and h_i can be determined by considering the equations at either the lower junction point, $q_{i,0}|_{p_i=q_{\min,i}}=q_{\min,i}$, and $dq_{i,0}/dp_i|_{p_i=q_{\min,i}}=0$ or those at the higher junction point, $q_{i,0}|_{p_i=q_{\max,i}}=q_{\max,i}$, and $dq_{i,0}/dp_i|_{p_i=q_{\max,i}}=0$.

For La, we can assume that $q_{\min,i}=0$ and $q_{\max,i}=3$. Plot of Eq. (19) is shown in Fig. 3. It can be seen that $q_{i,0}$ is bounded between 0 and 3 when p_i is below 0 or above 3 and $q_{i,0}$ approximately equals p_i in the middle range.

We can now show that with the $q_{i,0}$ defined by Eq. (19), this model predicts zero charges for any metallic or covalent

TABLE I. EIM parameters.

Species-dependent, charge-related parameters									
i	γ_i (V)	J_i (V e^{-1})	$q_{\min,i}$ (e)	$q_{\max,i}$ (e)	ξ_i (Å^{-1})	ζ_i	$r_{c,i}^*$ (Å)	g_i	h_i
La	28.38	7.484 66	0	3	0.9	0.025	6.0	3/2	−2/9
Br	−9.98	7.697 94	−1	0	0.9	0.025	6.0	3/2	−2

Pair-dependent, non-charge-related parameters							Universal
ij	$E_{b,ij}$ (eV)	α_{ij} (Å^{-1})	β_{ij} (Å^{-1})	$r_{e,ij}$ (Å)	$r_{c,ij}$ (Å)	κ_{ij} (Å^{-1})	
LaLa	−0.799 91	2.299 536	1.642 526	3.827 62	6.0	1.2	
BrBr	−0.469 56	1.276 460	0.981 892	4.375 36	5.4	1.2	s=1.644 98
LaBr	−5.810 34	8.210 592	$5.034\,371\times10^{-7}$	4.797 16	5.3	0.574 025	

systems where atoms are either all cations or all anions. For example, assume that all atoms in the system are cations. Any local site in the system will then have a positive-ion propensity. This means that any atoms embedded into the site should have a tendency to become negatively charged [Eq. (18)]. However, the charge range $q_{\min,i}$, $q_{\max,i}$ of a cation atom is defined in a positive range. As a result, the charge becomes zero [Eq. (19)].

Substituting Eq. (19) into Eq. (17), we have an analytical expression for the embedding energy as a function of ion propensity,

$$E_{\mathrm{emb},i}(\sigma_i) = \zeta_i\left[\frac{1}{2}J_i q_{i,0}^2(\sigma_i) + \sigma_i q_{i,0}(\sigma_i)\right], \qquad (20)$$

where $q_{i,0}$ is viewed as a function of ion propensity σ_i. Equation (20) can be used in Eq. (5) to calculate the total energy of the system.

III. PARAMETRIZATION

La exists in the $P6_3/mmc$ (hcp) phase at room temperature but transforms to a $Fm3m$ (fcc) phase at 200 °C or above.[63,64] Since our purpose is to study the mechanical behavior of the $LaBr_3$ compound during its synthesis at high temperatures, fcc La phase is assumed. The experimentally observed $P6_3/m$ (UCl_3 type) crystal[63] is used to model the $LaBr_3$ phase. The Br phase is an I_2 molecular crystal, so we approximated its atomic crystal using an fcc structure. Experimental lattice constants were taken from Refs. 63 and 46 for La and $LaBr_3$, respectively. The target lattice constant of the Br phase was estimated from its known material density of 3.119 g cm^{-3}. Following the previous approach,[35,65] we derived the cohesive energies of La, Br, and $LaBr_3$ phases from the experimental thermochemical data of various substances.[66] Based on the Pauling[67] and Mulliken[68] scales of electronegativity, we estimated the parameter γ_i (i =La,Br). The equilibrium charge at relaxed $LaBr_3$ lattice was assumed to be 90% of the maximum charge (maximum charges are defined as $q_{\max,\mathrm{La}}=3e$ and $q_{\min,\mathrm{Br}}=-1e$) as commonly done with the variable charge models.[35,39] We parametrize our EIM potential by optimizing its prediction of equilibrium charge, cohesive energy, and lattice constants against the corresponding values either from experiments or from our best estimates. In addition, we also require that the forces on Br atoms in the $LaBr_3$ structure be zero during parametrization because these forces are not naturally balanced.

An objective function was defined as a weighted sum of square deviation of predicted properties from the corresponding target values for all the three structures being fitted. With proper bounds for all parameters, optimization is done using four built-in methods of MATHEMATICA software (Ref. 69)—differential evolution, simulated annealing, default, and Nelder-Mead algorithms—and the results that gave the minimum objective function were used. We found that the four methods usually resulted in similar results, indicating that the objective function has a well-defined minimum. The parameters thus obtained are shown in Table I. One thing to note from Table I is that even at $\alpha_{\mathrm{LaBr}}/\beta_{\mathrm{LaBr}}\approx 1.6\times10^7$, we still get a smooth pair potential between La and Br (see Sec. IV). This indicates that the cutoff function [Eq. (8)] greatly increases the parameter range of Eq. (7) because the standard Morse potential works reasonably well only when the α/β value is close to 2.

IV. CHARACTERIZATION

In this section, we present characteristics of the EIM potential including the curves of the EIM functions, a comparison between the predicted and target properties, lattice energies, charge-related energy contributions to the lattice energies, and reactivity of the potential.

A. EIM functions

To characterize the fitted potential, the pair energy, the ion propensity, and the embedding energy defined by Eqs. (6), (15), and (20) are shown, respectively, in Figs. 4(a)–4(c). It can be seen from Fig. 4(a) that all the pair functions are very smooth and are cut off very nicely. Figure 4(b) shows that

TABLE II. Comparison between predicted and target values of lattice constants (a and c) and cohesive energy (E_c). Values in parenthesis are target values.

Structures	Lattice constants (Å)		E_c (eV/atom)
	a	c	
La	5.307		−4.478
	(5.307)		(−4.446)
Br	5.542		−1.308
	(5.541)		(−1.146)
$LaBr_3$	7.990	4.512	−4.305
	(7.965)	(4.512)	(−4.317)

(cation) La atoms create a positive-ion propensity and the magnitude of the ion propensity is increased when the distance from the La atoms is decreased; whereas (anion) Br atoms create a negative-ion propensity and the magnitude of the ion propensity is also increased when the distance from the Br atoms is decreased. Figure 4(c) indicates that when a La atom is embedded in a cation environment with a positive-ion propensity, the embedding energy is zero; whereas when it is embedded in an anion environment with a negative-ion propensity, it introduces an embedding energy due to the chemical reaction (ionization). Likewise, an embedded Br atom does not introduce embedding energy unless it is embedded in a cation environment. These potential functions, therefore, capture the basic requirement of our variable charge model defined above [assumption (c)]. This ensures a zero charge-related energy when the model is used for any metallic alloys or covalent compounds where no ionization conceptually occurs.

B. Predicted and target properties

Relaxed lattice constants and cohesive energy were calculated for the fcc crystal of the La and Br structures and the UCl_3 crystal of the $LaBr_3$ structure. The calculated lattice constants and cohesive energy are shown in Table II, along with the corresponding target values in parenthesis. It can be seen that the predicted lattice constants and cohesive energy are generally in good agreement with the target values. Since our intent is to model the $LaBr_3$ compound, it is more important to ensure that our model predicts a negative heat of mixing for $LaBr_3$ (i.e., the $LaBr_3$ structure is stable). From the cohesive energies of the La, Br, and $LaBr_3$ phases, we can get the heat of mixing of the $LaBr_3$ phase as $(4E_{c,LaBr_3} - E_{c,La} - 3E_{c,Br})/4 = -2.205$ eV/atom. The $\{11\bar{2}0\}$ surface energy was also calculated and found to be 0.052 eV/Å^2.

The calculated elastic constants are summarized in Table III. We did not have appropriate target values for elastic constants other than the *ab initio* bulk modulus for La.[70] As a result, we did not fit them but rather constrain them to ensure the mechanical stability for all the phases fitted, as shown in Table III.

C. Lattice energies and reactivity

We further explore the behavior of the potential on predicting the system energy as the crystal is compressed and stretched. The energy per atom as a function hydrostatic strain is shown in Fig. 5 for the (fcc) La, (fcc) Br, and (UCl_3) $LaBr_3$ phases. Again smooth curves can be seen. These curves nicely decay to zero when the lattices are stretched.

To examine contributions from the charge-related energies, we plot in Fig. 6 the total embedding energy (per atom) as a function of hydrostatic strain for the La, Br, and $LaBr_3$ phases. It can be seen that this charged-related energy is constantly zero for the La and Br phases, indicating that there is no ionization reaction in these systems. However, Fig. 6 also shows that a charge-related energy contribution becomes significant when La and Br atoms in the $LaBr_3$ are brought close. The potential therefore can capture the reactive ionization of the system.

The environment dependence of the bonding can be demonstrated by considering a pair of La atoms separated by a

TABLE III. Single-crystal elastic constants (eV/Å^3). *Ab initio* data (Ref. 70) are given in parentheses.

Cubic bulk and shear moduli						
	B		C'		C_{44}	
La	0.999(0.206)		0.274		0.816	
Br	0.371		0.139		0.278	
Hexagonal elastic constants C_{ij}						
	ij	1	2	3	4	5	6
$LaBr_3$	1	1.393	0.903	0.469	0.000	0.000	0.000
	2	0.903	1.442	0.903	0.000	0.000	0.000
	3	0.469	0.903	1.393	0.000	0.000	0.000
	4	0.000	0.000	0.000	0.903	0.000	0.000
	5	0.000	0.000	0.000	0.000	0.462	0.000
	6	0.000	0.000	0.000	0.000	0.000	0.903

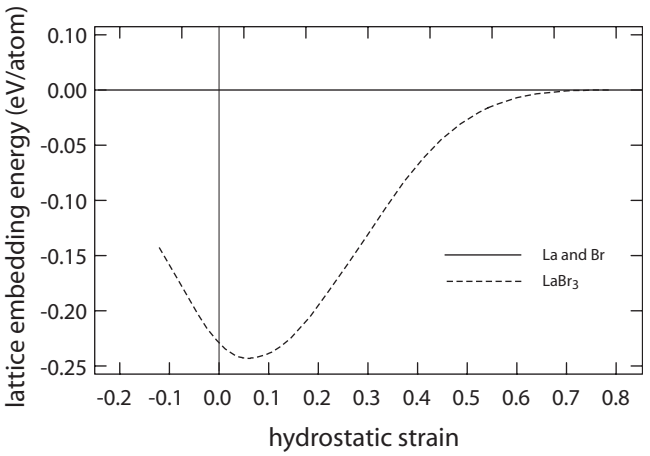

FIG. 6. Charge-related lattice energies for the (fcc) La, (fcc) Br, and (UCl_3) $LaBr_3$ phases.

distance r. Assume that such a pair of atoms is embedded into a uniform medium with an ion propensity of σ_0. The total ion propensity at the La site then becomes $\sigma_0+\sigma^a_{\mathrm{La}}(r)$. This ion propensity may induce a charge on the La atoms as can be calculated using Eqs. (14) and (15). The energy of the system can be expressed as $E=\phi_{\mathrm{LaLa}}(r)+2E_{\mathrm{emb,La}}[\sigma_0+\sigma^a_{\mathrm{La}}(r)]$. The force between the two La atoms is then defined by $f=-dE/dr$. Assume that the distance between the two La atoms is $r=3.5$ Å. The charge on the La atoms and the force between the two La atoms were calculated as a function of the background parameter σ_0. The results of the calculated charge and force are shown in Figs. 7(a) and 7(b), respectively. It can be seen that when the background ion propensity σ_0 is large, no charge is induced on the La atoms and the force between the two atoms is a constant that is entirely defined by the pair energy $\phi_{\mathrm{LaLa}}(r)$. As the background ion propensity is decreased to a large negative value, a positive charge is induced on the La atoms [Fig. 7(a)]. As a result, an additional repulsive force is introduced between the two La atoms [Fig. 7(b)]. At very large negative-ion propensity, the charge on the La atoms is saturated at $+3e$. As a result, the repulsive force is also saturated. The model, therefore, captures the physical mechanisms described in Fig. 1.

D. Lattice geometry of the $LaBr_3$ crystal

Energy minimization was used to relax the $LaBr_3$ crystal so that the geometry of the lattice can be seen. Figures 8(a) and 8(b) show, respectively, the experimental and the predicted {0001} view of the atomic configurations of the $LaBr_3$ crystal, where the bigger orange balls represent La atoms whereas the smaller gray balls represent Br atoms. The key feature of the $LaBr_3$ structure is that each La atom is coordinated with nine Br atoms—three on a plane containing the La, three below, and three above—defining a tricapped trigonal prism. Experiments show that the length of the three La-Br bonds coplanar with La is about 3.156 Å whereas that of the remaining six La-Br bonds is 3.095 Å [Fig. 8(a)]. The predicted lengths for the two bonds are 3.159 and 3.094 Å. It can be seen that not only the values are close, but both experiments and simulations show that the length for the on-plane bonds is slightly longer than that of the off-plane bonds.

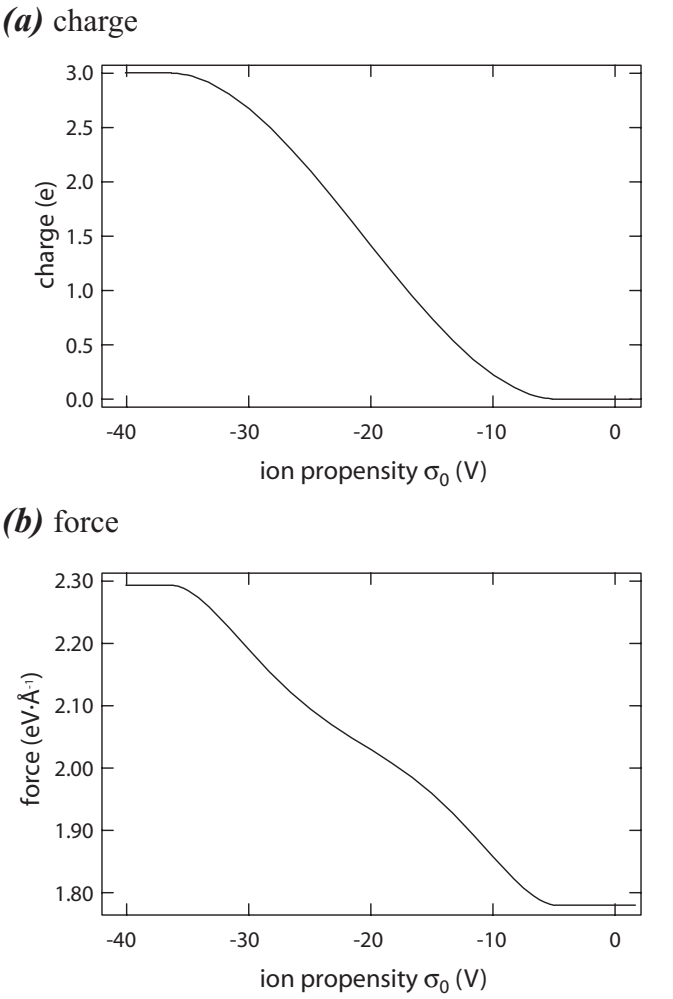

FIG. 7. Effects of background ion propensity on the charge and the force of the two La atoms separated by a distance of 3.5 Å. (a) Charge and (b) force.

V. MOLECULAR-DYNAMICS SIMULATIONS

We first examine energy conservation during MD simulations. A bulk UCl_3 type of $LaBr_3$ crystal containing 896 atoms was used. A simulated annealing was carried out at 600 K for a nanosecond using a time step size of 0.001 ps. The calculated average relative energy change per atom is shown in Fig. 9 as a function of time. It can be seen that the system energy remained almost constant over a relatively long time of a nanosecond. The EIM thus resolves the problem of the conventional variable charge potential shown in Fig. 2.

We now explore the mechanical behavior of the $LaBr_3$ crystal under a simulated tensile test. A $LaBr_3$ crystal with $[\bar{1}100]$ x axis, $[0001]$ y axis, and $[\bar{1}\bar{1}20]$ z axis was used. The crystal dimension is about $32\times27\times28$ Å^3, with periodic boundary conditions in all the three coordinate directions. Molecular-dynamics simulations of tensile test along the z axis were then carried out by uniformly stretching the system

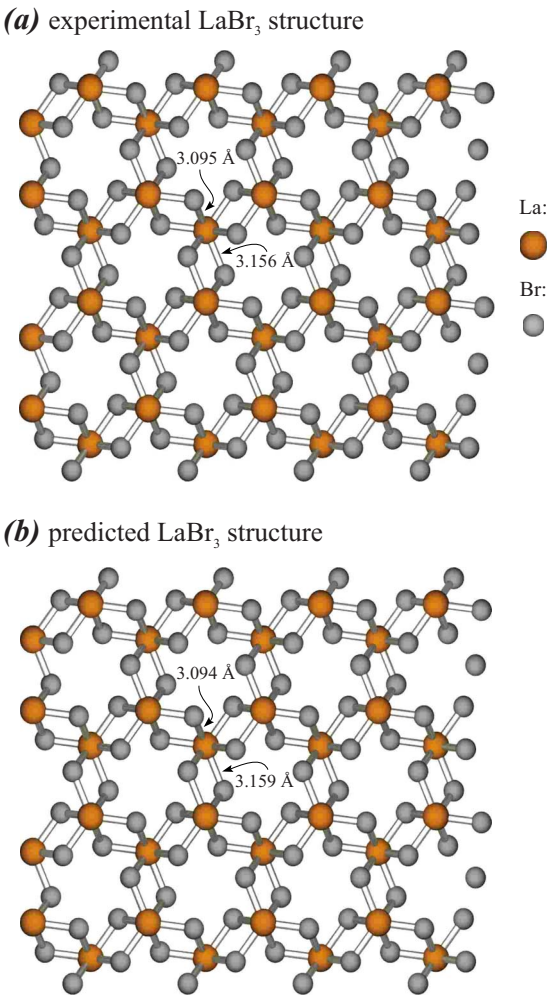

FIG. 8. (Color online) {0001} view of the $LaBr_3$ lattice. (a) Experimental measurement (Ref. 46) and (b) atomistic simulation.

in the z direction using an average strain rate of about 3.0×10^{10}/s, whereas the dimensions in the x and y directions remained constant. The initial temperature was set at 300 K and no temperature control was applied during the simulations. The x-z view of the system before and after a 0.25 strain is shown, respectively, in Figs. 10(a) and 10(b). It can

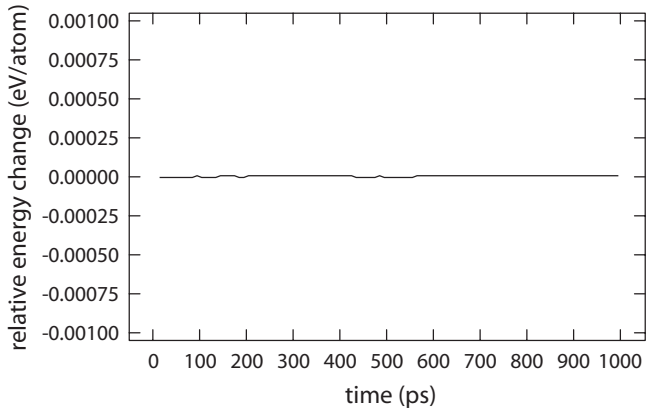

FIG. 9. Relative energy change (per atom) as a function of time predicted by the EIM.

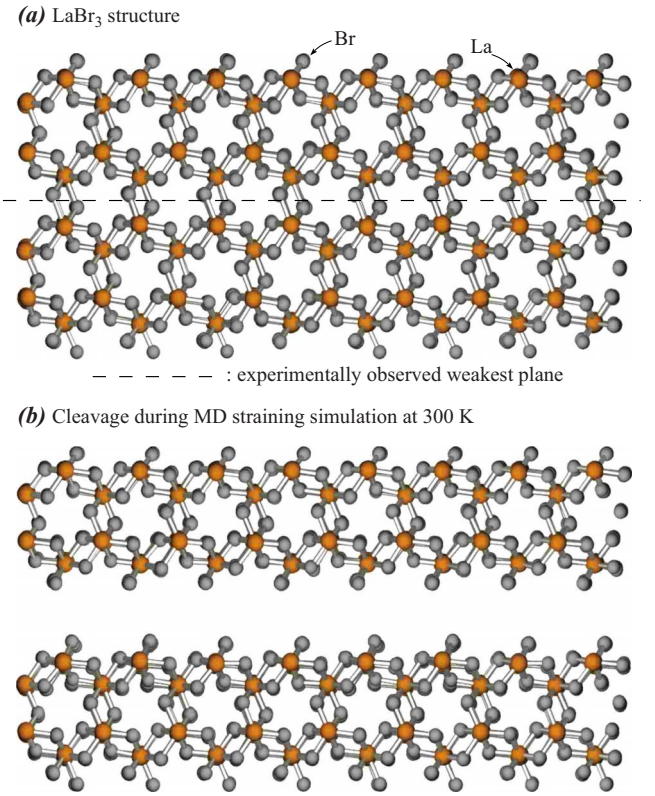

FIG. 10. (Color online) Molecular-dynamics simulation of a tensile test along the $[\bar{1}\bar{1}20]$ direction of a $LaBr_3$ crystal at a strain rate of about 3.0×10^{10}/s and a temperature of 300 K. (a) Before strain and (b) after a strain of about 0.25.

be seen that the system underwent a clear cleavage along the $(11\bar{2}0)$ plane, thereby capturing a key phenomenon of the material.

Average atomic stresses based on the Virial theorem[71] were used to estimate global tensile stress along the z direction. Stress vs strain curves were calculated for two tensile tests carried out at strain rates of 3.0×10^{10}/s and 1.3×10^{10}/s, and the results are shown in Fig. 11. It can be seen that both strain rates produced almost identical results. Initially the sample underwent a linear elastic deformation when the strain is applied. Young's modulus estimated from

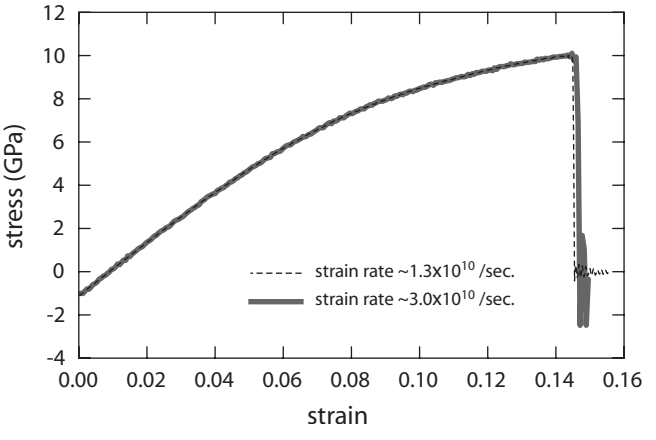

FIG. 11. Stress as a function of strain.

the figure is about 118 GPa. An abrupt complete fracture appeared at a strain around 0.144, signifying the cleavage. As expected from a defect-free crystal, a very high fracture strength of around 10 GPa was predicted.

VI. CONCLUSIONS

A computationally efficient embedded-ion method interatomic potential has been proposed for any material systems that involve significant ionic interactions. This model captures the essential charge-transfer phenomena and the environment dependence of the ionic bonding. It is transferable to other metallic or covalent systems without modification of the interatomic potentials that are already developed for these systems. While the key physics of the previous charge-transfer potentials is retained, the EIM does not explicitly solve charges and therefore ensures the energy conservation without having to incorporate the charge derivatives in the force calculations. With an improved cutoff function, this model can be readily parametrized. Using the La-Br system as an example, we demonstrated that this model captured some key properties of the $LaBr_3$ compound including the crystal structure, lattice geometry, and the $\{11\bar{2}0\}$ cleavage. While we are working to improve the method by incorporating the dependence of embedding energy on ion propensities at neighboring atom sites and the associated charge conservation and to improve the parametrization by separating the charge-related component using more *ab initio* inputs, we feel that the current model can already provide a viable interatomic potential for nonstoichiometric ionic systems, which is simply lacking today.

ACKNOWLEDGMENTS

Sandia is a multiprogram laboratory operated by Sandia Corporation, a Lockheed Martin Corporation, for the National Nuclear Security Administration of the United States Department of Energy under Contract No. DEAC04-94AL85000. This project was sponsored by the U.S. Department of Energy, NA22 Advanced Materials.

*Corresponding author. FAX: 1 925 294 3410; xzhou@sandia.gov

[1] W. J. Gallagher and S. S. P. Parkin, IBM J. Res. Dev. **50**, 5 (2006).
[2] S. Okamoto and A. J. Millis, Nature (London) **428**, 630 (2004).
[3] Y. Tokura and N. Nagaosa, Science **288**, 462 (2000).
[4] S. Thiel, G. Hammerl, A. Schmehl, C. W. Schneider, and J. Mannhart, Science **313**, 1942 (2006).
[5] M. M. Qazilbash, M. Brehm, B. G. Chae, P. C. Ho, G. O. Andreev, B. J. Kim, S. J. Yun, A. V. Balatsky, M. B. Maple, F. Keilmann, H. T. Kim, and D. N. Basov, Science **318**, 1750 (2007).
[6] H. Ohta, K. S. Kim, Y. Mune, T. Mizoguchi, K. Nomura, S. Ohta, T. Nomura, Y. Nakanishi, Y. Ikuhara, M. Hirano, H. Hosono, and K. Koumoto, Nature Mater. **6**, 129 (2007).
[7] A. Ohtomo and H. Y. Hwang, Nature (London) **427**, 423 (2004).
[8] N. Reyren, S. Thiel, A. D. Caviglia, L. F. Kourkoutis, G. Hammerl, C. Richter, C. W. Schneider, T. Kopp, A. S. Ruetschi, D. Jaccard, M. Gabay, D. A. Muller, and J. M. Triscone, Science **317**, 1196 (2007).
[9] W. W. Moses, Nucl. Instrum. Methods Phys. Res. A **487**, 123 (2002).
[10] W. M. Higgins, A. Churilov, E. van Loef, J. Glodo, M. Squillante, and K. Shah, J. Cryst. Growth **310**, 2085 (2008).
[11] X. W. Zhou, H. N. G. Wadley, R. A. Johnson, D. J. Larson, N. Tabat, A. Cerezo, A. K. Petford-Long, G. D. W. Smith, P. H. Clifton, R. L. Martens, and T. F. Kelly, Acta Mater. **49**, 4005 (2001).
[12] X. W. Zhou, H. N. G. Wadley, and D. X. Wang, Comput. Mater. Sci. **39**, 794 (2007).
[13] X. W. Zhou and H. N. G. Wadley, Phys. Rev. B **71**, 054418 (2005).
[14] F. Hutchinson, M. Wilson, and P. A. Madden, J. Phys.: Condens. Matter **12**, 10389 (2000).
[15] M. S. Daw and M. I. Baskes, Phys. Rev. B **29**, 6443 (1984).
[16] S. M. Foiles, M. I. Baskes, and M. S. Daw, Phys. Rev. B **33**, 7983 (1986).
[17] X. W. Zhou, R. A. Johnson, and H. N. G. Wadley, Phys. Rev. B **69**, 144113 (2004).
[18] J. Tersoff, Phys. Rev. B **37**, 6991 (1988).
[19] J. Tersoff, Phys. Rev. B **39**, 5566(R) (1989).
[20] K. Albe, K. Nordlund, J. Nord, and A. Kuronen, Phys. Rev. B **66**, 035205 (2002).
[21] D. A. Murdick, X. W. Zhou, and H. N. G. Wadley, Phys. Rev. B **72**, 205340 (2005).
[22] R. Drautz, D. A. Murdick, D. Nguyen-Manh, X. W. Zhou, H. N. G. Wadley, and D. G. Pettifor, Phys. Rev. B **72**, 144105 (2005).
[23] R. Drautz, X. W. Zhou, D. A. Murdick, B. Gillespie, H. N. G. Wadley, and D. G. Pettifor, Prog. Mater. Sci. **52**, 196 (2007).
[24] D. G. Pettifor, M. W. Finnis, D. Nguyen-Manh, D. A. Murdick, X. W. Zhou, and H. N. G. Wadley, Mater. Sci. Eng., A **365**, 2 (2004).
[25] D. A. Murdick, X. W. Zhou, H. N. G. Wadley, D. Nguyen-Manh, R. Drautz, and D. G. Pettifor, Phys. Rev. B **73**, 045206 (2006).
[26] S. R. Phillpot, S. B. Sinnott, and A. Asthagiri, Annu. Rev. Mater. Res. **37**, 239 (2007).
[27] M. Baudin and K. Hermansson, Surf. Sci. **474**, 107 (2001).
[28] B. G. Dick and A. W. Overhauser, Phys. Rev. **112**, 90 (1958).
[29] A. Dwivedi and A. N. Cormack, Philos. Mag. A **61**, 1 (1990).
[30] P. J. D. Lindan and M. J. Gillan, J. Phys.: Condens. Matter **5**, 1019 (1993).
[31] G. V. Lewis and C. R. A. Catlow, J. Phys. C **18**, 1149 (1985).
[32] M. S. Khan, M. S. Islam, and D. R. Bates, J. Mater. Chem. **8**, 2299 (1998).
[33] C. R. A. Catlow, J. Chem. Soc., Faraday Trans. **86**, 1167 (1990).
[34] M. R. Levy, A. Patel, C. R. Stanek, K. McClellan, and R. W. Grimes, Phys. Status Solidi C **4**, 1226 (2007).
[35] X. W. Zhou, H. N. G. Wadley, J.-S. Filhol, and M. N. Neurock, Phys. Rev. B **69**, 035402 (2004).
[36] T. Campbell, R. K. Kalia, A. Nakano, P. Vashishta, S. Ogata, and S. Rodgers, Phys. Rev. Lett. **82**, 4866 (1999).

[37] S. Ogata and T. J. Campbell, J. Phys.: Condens. Matter **10**, 11449 (1998).
[38] Y. Ma and S. H. Garofalini, J. Chem. Phys. **128**, 084505 (2008).
[39] F. H. Streitz and J. W. Mintmire, Phys. Rev. B **50**, 11996 (1994).
[40] A. K. Rappe and W. A. Goddard, J. Phys. Chem. **95**, 3358 (1991).
[41] S. W. Rick, S. J. Stuart, and B. J. Berne, J. Chem. Phys. **101**, 6141 (1994).
[42] H. B. Schlegel, S. S. Lyengar, X. Li, J. M. Millam, G. A. Voth, G. E. Scuseria, and M. J. Frisch, J. Chem. Phys. **117**, 8694 (2002).
[43] J. M. Herbert and M. Head-Gordon, Phys. Chem. Chem. Phys. **7**, 3269 (2005).
[44] A. M. N. Niklasson, C. J. Tymczak, and M. Challacombe, J. Chem. Phys. **126**, 144103 (2007).
[45] J. M. Herbert and M. Head-Gordon, J. Chem. Phys. **121**, 11542 (2004).
[46] K. Kramer, T. Schleid, M. Schulze, W. Urland, and G. Meyer, Z. Anorg. Allg. Chem. **575**, 61 (1989).
[47] W. H. Zachariasen, Acta Crystallogr. **1**, 265 (1948).
[48] V. M. Goldschmidt, *Geochemisce Verterlungsgesetze der Elemente* (Norske Videnskap, Oslo, 1927).
[49] A. S. Bhalla, R. Guo, and R. Roy, Mater. Res. Innovations **4**, 3 (2000).
[50] L. Pauling, *The Nature of the Chemical Bond*, 2nd ed. (Cornell University Press, Ithaca, 1945), p. 164.
[51] R. T. Sanderson, J. Chem. Phys. **23**, 2467 (1955).
[52] R. P. Iczkowski and J. L. Margrave, J. Am. Chem. Soc. **83**, 3547 (1961).
[53] Liu Liang, Lu Wencong, and Chen Nianyi, J. Phys. Chem. Solids **65**, 855 (2004).
[54] F. Reif, *Fundamentals of Statistical and Thermal Physics* (McGraw-Hill, New York, 1965).
[55] A. Prince, *Alloy Phase Equilibria*, (Elsevier, Amsterdam, 1966).
[56] A. S. Richard, *Thermodynamics of Solids* (Wiley, New York, 1972).
[57] X. W. Zhou and H. N. G. Wadley, J. Phys.: Condens. Matter **17**, 3619 (2005).
[58] A. C. T. van Duin, S. Dasgupta, F. Lorant, and W. A. Goddard III, J. Phys. Chem. A **105**, 9396 (2001).
[59] D. E. Parry, Surf. Sci. **49**, 433 (1975).
[60] D. M. Heyes, Surf. Sci. Lett. **293**, L857 (1993).
[61] J. Tersoff, Phys. Rev. B **37**, 6991 (1988).
[62] J. Tersoff, Phys. Rev. B **39**, 5566 (1989).
[63] J. D. H. Donnay and H. M. Ondik, *Crystal Data, Determinative Tables: Inorganic Compounds*, 3rd ed., (U.S. Department of Commerce, National Bureau of Standards, and Joint Committee on Power Diffraction Standards, Swarthmore, PA, 1973), Vol. 2.
[64] D. Zamir and D. S. Schreiber, Phys. Rev. **136**, A1087 (1964).
[65] X. W. Zhou, J. A. Zimmerman, B. M. Wong, and J. J. Hoyt, J. Mater. Res. **23**, 704 (2008).
[66] I. Barin, *Thermochemical Data of Pure Substances* (VCH, Weinheim, 1993).
[67] L. Pauling, J. Am. Chem. Soc. **54**, 3570 (1932).
[68] R. S. Mulliken, J. Chem. Phys. **2**, 782 (1934).
[69] Wolfram Research, Inc., 2007 (http://www.wolfram.com/products/mathematica/index.html).
[70] D. Singh, Phys. Rev. B **43**, 6388 (1991).
[71] J. Zimmerman, E. Webb III, J. Hoyt, R. Jones, P. Klein, and D. Bammann, Modell. Simul. Mater. Sci. Eng. **12**, S319 (2004).